NTNU – Trondheim
Norwegian University of
Science and Technology

Modeling and Simulation of a flexible Damper during Ice in Propeller Impacts

Alexandra Beckenkamp

Marine Technology
Submission date: June 2015
Supervisor: Eilif Pedersen, IMT

Norwegian University of Science and Technology
Department of Marine Technology

Preface

This thesis is written to finalize the international master program in marine technology (MSN 1) at the Norwegian University of Science and Technology – NTNU in Trondheim. The thesis was written autonomous with the support of the supervisor Eilif Pedersen.
The thesis shows the modeling of a given flexible coupling with the use of bond graphs, investigates the behavior of the model and discusses it's suitability for ice load cases. The intention is to find a suitable coupling model for the simulation of drive trains in arctic conditions.

Contents

List of Figures

List of Tables

Scope of work

Master thesis, Spring 2015

Modeling and simulation of flexible dampers during ice in propeller impacts

There has been an increase in ship traffic in Arctic waters in the last years. This challenges today's ship design. One of the challenges is the contact loads that occur due to ice blocks encountering the ship propeller. The ice-propeller interaction is a complicated process and more knowledge on the effect of this interaction on the ship propulsion drive train is needed. This master thesis focuses on improving the dynamic mathematical model of one of the ship propulsion drive train components, namely the flexible coupling, during peak loads.

- Develop a mathematical model of the Geislinger flexible coupling using the bond graph approach. The model should include the effects of the radially aligned spring and the oil transfer between the oil chambers. The model is to be implemented in the 20-sim simulation software.
- Compare the model to the empirically found dynamic stiffness and damping provided by the coupling manufacturer.
- Investigate the effect of changing the model parameters on the dynamic stiffness and damping.
- Implement the mathematical model of the Geislinger coupling into a marine propulsion drive train, where the propeller is to be subjected by representative ice propeller interaction loads.
- Compare the drive train model including the mathematical model of the Geislinger flexible coupling to existing model.

Deadline: 10. June 2015
Supervisor: Eilif Pedersen

Abstract

In the beginning the problematic of ice impacts on a ships drive train and the similarity of this work to last year's thesis from Bjørn Eliassen Vik is mentioned. After that the Bond-Graph-Methodology on which this thesis is based in shortly explained. Then the modeling of the coupling is explained. Here the coupling is divided into parts and modeled separately. A particular interest is on the dynamic behavior of the springs. These parts are then joined together. In the next chapter the coupling model is compared to the values given by the manufacturer. It shows that the model is too stiff. Therefore the thickness of the springs and the bulk-modulus of the oil is adjusted until it matches the template.
The model is than tested by varying the excitation frequency, the resistance of the load and the inertia of the coupling. It shows that the frequency has a great influence on the stiffness of the system, the resistance a limited influence and the inertia an influence on the nominal frequency of the system.
In the end the coupling is inserted into a drive train model. First it is simulated in open water, than an additional ice load is placed upon the propeller. The results are compared to simulations of the drive train with a simpler coupling and without a coupling. The results show that both couplings have damping capabilities. However, the ice load is too little to determine the effect of sudden peak loads properly.

Chapter 1

Introduction

1.1 Background

Shipping in ice waters leads to many stresses on vessels. One area of interest is the effect of propeller-ice impacts on the vessels' propulsion train. The impact of the propeller blades on ice leads to vibration peaks in the shaft which can transmit to the bearings and the engine [Polic, 2013]. To avoid damage to the engine, flexible couplings are used to stop the transmission of vibrations through the shaft. However, these coupling are usually designed for regular smaller vibrations [Polic, 2013] and there is not much knowledge about the behavior of flexible couplings during peak vibration loads.

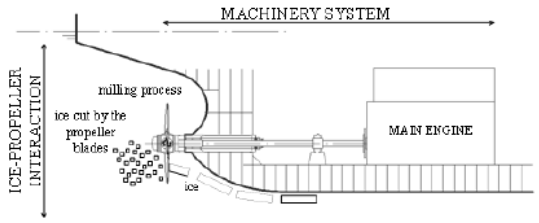

Figure 1.1: Impact of ice on propulsion machinery [Polic, 2013]

1.2 Comparison to previous work

This thesis has the same scope as the thesis of Bjørn Eliassen Vik from 2014 with the title "Development and Verification of a Gesilinger [sic] Flexible Coupling Bond Graph Model". However, the bond graph model described in this thesis was developed from scratch. To maintain some comparability between the works, some input values used in Mr. Vik's thesis were verified and adopted. The ice motion model was adopted from the same source.

1.3 Structure

The behavior of a flexible coupling during ice induced vibrations will be simulated in the following chapters. A coupling from the manufacturer Geislinger will be taken as an example. A model of the coupling will be made with the Bond Graph method. Then the model will be implemented into the simulation program 20-sim. The model will then be subjected to a load input which simulates the effect of the engine and the propeller. The resulting behavior of the model will then be investigated.

Chapter 2

Methods

2.1 Bond Graphs

The coupling in this thesis is modeled with the bond graph method, a modeling technique for various dynamic systems. It can be used for mechanical, hydraulic, electrical, thermal systems and any combination of these systems. It is convenient for the present coupling due to the mainly mechanical system that is combined with oil chambers for damping [Geislinger, 2014]. The method was invented by Henry Paynter in 1959 and further developed by him and his Ph.d. students Dean Karnopp and Ronald Rosenberg [Borutzki, 2000]. For this method the system is divided into ideal objects that represent the physical properties of the model. The elements are [Borutzki, 2000]:

- Energy sources and sinks (Source = Sf &Se)
- Energy storage (Capacitor = C, Inertia = I)
- Energy consumers (Resistor = R)
- Ideal couplings and transformers (Transformer = TF, Gyrator = GY)
- Ideal power distributors (Bonds, 0- and 1-junctions)

These elements are linked by bonds that represent the energy transfer between them. The way the elements interact is further defined by formulas that can be inserted into them. They are used to modify the given relations and represent the physical dependencies.

2.2 20-sim

The program used to simulate the model is 20-sim. That is a self-contained commercial program developed by Controllab Products [Controllab, 2015]. It can be used to simulate bond graphs as well as block- and iconic diagrams. The version used for this Thesis is 4.5.

Chapter 3

System

3.1 Coupling

The coupling used in this thesis is a BC 110/10/45 UC/L type from Geislinger GmbH. This stands for [Geislinger, 2014]:

- BC – type of connection flanges
- 110 – outer diameter of center part [cm]
- 10 – width of spring pack [cm]
- 45 – stiffness series, approx. twist at nominal torque [mrad]
- UC – reversible
- L – left hand rotation

The driving wheel of this coupling is the outer wheel. It is connected to the driven inner wheel by a number of flat springs that transmit the power. The springs are fixed to the outer wheel and reach into grooves within the inner wheel. The twist is limited to 0.07rad in both turn directions by a bumper. The coupling and the springs are made out of steel. Between the springs and the bumper are oil filled chambers. The chambers on both sides of the bumper are connected by a small orifice (ΔK) between the tip of the bumper and the inner wheel. The oil is the regular system oil of the engine and is not additionally pressurized.

3.2 Propulsion Chain

To simulate the response of the coupling to the vibrations induced from the engine and the propeller, it is imbedded into a modeled propulsion chain. The engine model was provided by Eilif Pedersen. The archetype of the engine is unknown to the author. It is a 2-stroke diesel engine with 6-cylinders. The propeller shaft is considered to be much stiffer than the coupling. Therefore it is negligible and not included in the model. The propeller is modeled according to the power output of the engine.

3.3 Modeling of the coupling

The coupling can be divided into twelve equal sections. Each consists of two springs, one bumper and three oil chambers. The movement in each of the section is assumed to be uniform and rotational symmetric. Therefore every left oil chamber and spring behaves like their 11 counterparts. This is the same with the middle oil chamber as well as the right chamber and spring. Therefore the outer two chambers are connected through the groove under the bumper.
If possible, the coupling is regarded as a whole. However, to reduce the complexity of the model, only one section of the springs and the oil system is modeled. This reduction needs to be counterbalanced when the model is assembled.

3.4 Outer and Inner wheel

The inner and outer wheels are each rotating masses. Therefore, they are represented by a 1-junction with an I-element for the inertia. The Inertia is given in the product catalogue with 385kgm^2 for the outer wheel and 21.7kgm^2 for the inner wheel [Geislinger, 2014].

3.5 Springs

3.5.1 Structure

One end of each spring is mounted into the outer ring of the coupling in a fixed bearing. The other end reaches into a grove in the inner ring as a floating bearing. If the outer wheel is turned, the spring pushes the inner ring and

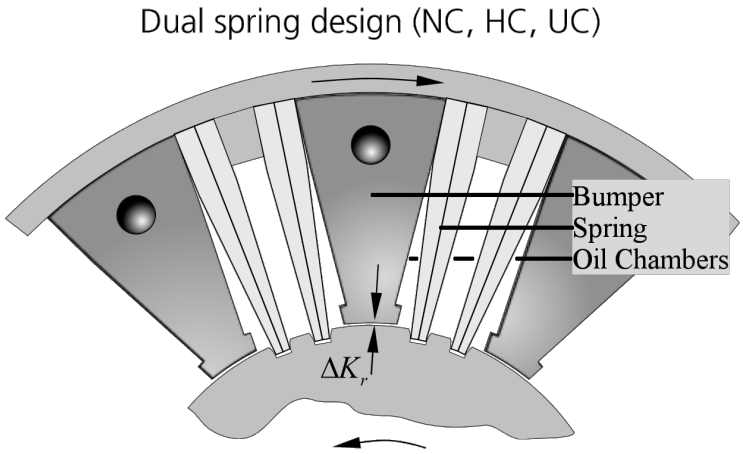

Figure 3.1: Two sections of the coupling [Geislinger, 2014]

gets bent due to the resulting force. It is assumed that the vibration modes of the stimulated spring have an influence on the model behavior. To model the dynamic behavior, the springs are seen as cantilevered beams with force acting on the tip of the beam. This is done according to the method described in [Karnopp, 2006]. The tapered shape of the springs is disregarded.

To model the dynamic response, each mode of vibration needs to be represented. For the input equations, the following differential equation needs to be solved [Karnopp, 2006]:

$$\frac{d^4Y}{dx^4} - k^4Y = 0 \tag{3.1}$$

The general solution for this equation is:

$$Y(x) = Asin(kx) + Bcos(kx) + Csinh(kx) + Dcosh(kx) \tag{3.2}$$

Since it is a cantilevered beam with force acting on the tip, the following boundary conditions apply:

$$\frac{dY(0)}{dx} = 0 \tag{3.3}$$

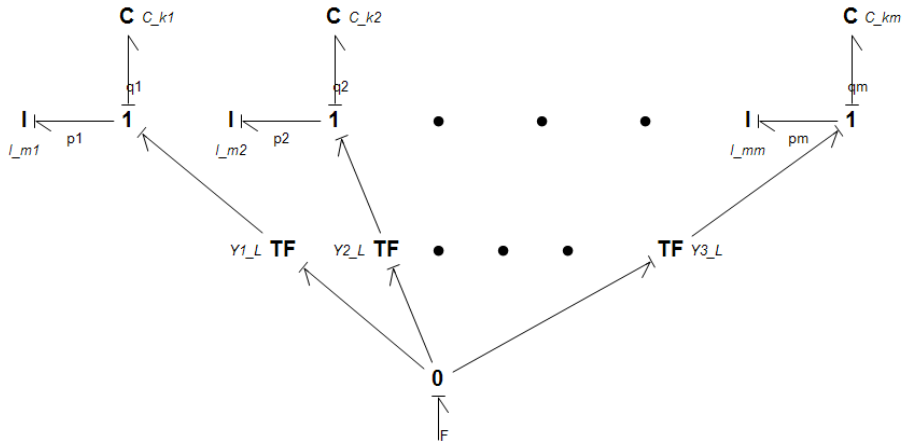

Figure 3.2: Modal vibration model [Karnopp, 2006]

$$\frac{d^2Y(0)}{dx^2} = 0 \tag{3.4}$$

$$\frac{d^3Y(L)}{dx^3} = 0 \tag{3.5}$$

$$\frac{d^4Y(L)}{dx^4} = 0 \tag{3.6}$$

Solving this according to [Meirovitch, 2001] leads to the following results:

The zero points for the equation

$$cos(x) \cdot cosh(x) + 1 = 0 \tag{3.7}$$

are

$$alfan = [1.875104069,\ 4.694091133,\ 7.854757435,\ 10.99554073,\ 14.13716839] \tag{3.8}$$

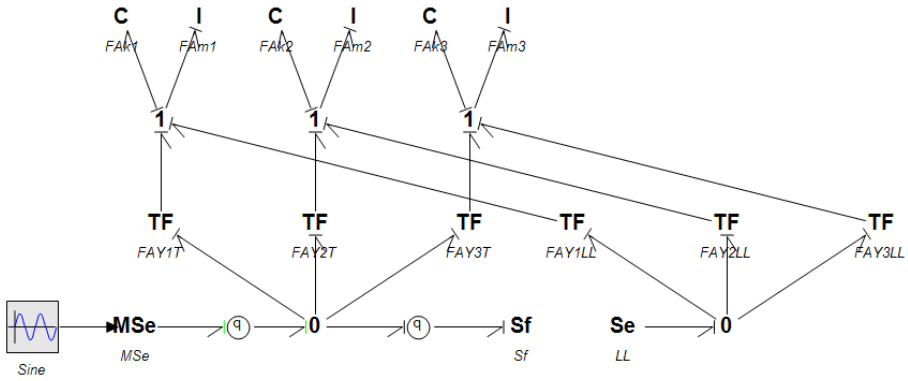

Figure 3.3: Bond Graph of spring with tip and line load

The ratio of coefficients is:

$$\frac{B}{A} = -\frac{sin(kL) + sinh(kL)}{cos(kL) + cosh(kL)} \tag{3.9}$$

The eigenfunction is:

$$Y_r(x) = A_r \left[sin(k_n x) - sinh(k_n x) - \frac{sin(k_n x) + sinh(k_n x)}{cos(k_n x) + cosh(k_n x)} (cos(k_n x) - cosh(k_n x)) \right] \tag{3.10}$$

The eigenfunction is then used as equation for the TF-element.
The effect of the oil pressure on the spring is modeled in the same way with a line load instead of a tip load. The resulting bond graph is shown in Figure 3.3.

3.5.2 Input

As an input for the I-element, the mass of the springs is calculated. The dimensions are taken from the manufacturer's drawings published in [Vik, 2014]. Since the springs are regarded as rectangular beams and not as cantilevered beams, the medium width is used. As material, spring steel 1.7108 is assumed. This gives an E-modul of 210GPa and a density of 7430kg/m² [DEW, 2015].

For the C-element the spring stiffness is calculated with the formulas given in [Karnopp, 2006]:

$$m_m = \frac{\rho \cdot A \cdot L}{2} \tag{3.11}$$

$$\omega_m = \sqrt{\frac{E \cdot I}{\rho \cdot A} \cdot \frac{(k_n \cdot L)^4}{L^4}} \tag{3.12}$$

$$k_m = m_m \cdot \omega_m^2 \tag{3.13}$$

And the second moment of Inertia from [Richard, 2008]:

$$I = \frac{h \cdot b^3}{12} \tag{3.14}$$

The dimensions of the spring are taken from [Vik, 2014].

3.6 Bumper

The bumper is designed to limit the twist equally in both directions. The maximum twist angle is 0.07rad. This is considered to be equal to a spring-damper system with a very short coil spring. The damper should only active when the spring moves into the bumper but not when it moves away from it. The model of the bumper is provided by Prof. Eilif Pedersen.
The damping factor is calculated with this formula [Meirovitch, 2001]:

$$c = 2 \cdot \zeta \cdot \sqrt{k \cdot m} \tag{3.15}$$

As a value for the mass, the weight of the outer wheel is used. This is m_{tot}=1870kg [Geislinger, 2014]. The decay of the oscillation is defined by ζ. For the author it seems most likely that the system is under damped. Therefore ζ=0.2 is chosen [Meirovitch, 2001]. The spring stiffness k is calculated with the following formula [Muhs, 2007]:

$$k = \frac{F}{\Delta s} \tag{3.16}$$

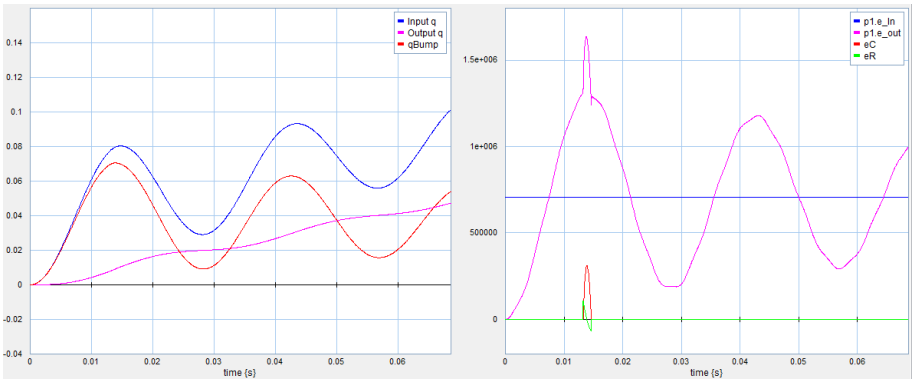

Figure 3.4: Bumper activation at 3.25xFn

As input force, the nominal torque of 218kN is chosen. Because there is no actual spring but rather a solid wall, the spring deflection is assumed to be only 0.1mm. This results in the following values:

- k= 6.108
- c= 61165

The bumper is tested by subjecting the coupling to a static excitation force. The oil is not included to isolate the behavior of the bumper. However, the bumper is not activated if the nominal force is applied. Therefore the excitation force is increased by the factor 3.25 to 708.5kNm.

The activation of the bumper can be seen in the spike of eC and eR at 0.015s.

3.7 Oil System

3.7.1 System

The oil system consists of three chambers per section. The upper and lower boundaries are the outer and inner ring respectively. They are divided by the springs and the bumper. Between the bumper and the inner ring is a clearance (ΔK) that allows a small oil flow between the chambers on both sides of

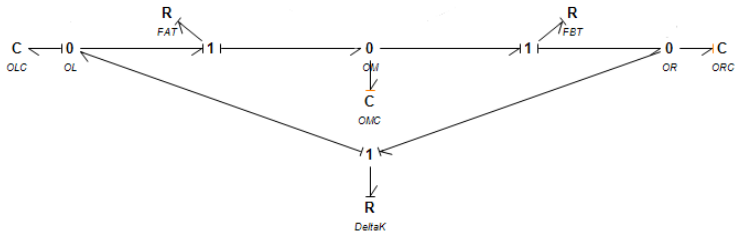

Figure 3.5: Oil system model

the bumper. The springs end in a groove in the inner ring. This divides the chambers. An oil flow at this location is not mentioned by the manufacturer [Geislinger, 2014] and therefore not assumed in this model. There is no significant angular speed difference between the outer and the inner wheel. Therefore the friction forces between the wheels and the oil are disregarded. The three chambers are each represented by a 0-junction to account for their possibly different pressure. The oil is assumed to be slightly compressible. Therefore a C-element is added to the 0-junction. The clearance (ΔK) is considered to be a valve with a small diameter. This is represented by the R-element. The direction of the power bonds between the outer oil chambers and the orifice is into the positive turn direction of the wheel.

3.7.2 Input

Because of the compressibility of the oil, the volume is calculated with the dimensions of the coupling. Then the k-value is determined by the following formula [Pedersen, 2010]:

$$k = \frac{V}{\beta} \tag{3.17}$$

With the bulk modulus β=1.5GPa for mineral oil [Watter, 2013]. The clearance (ΔK) resistance is calculated with the following formula [Pedersen, 2010]:

$$\dot{V} = \zeta \cdot A \sqrt{\frac{2}{\rho} \cdot \Delta P_v} \tag{3.18}$$

As input value for the pressure difference ΔP, the effort input into the R-element is used and for the Volume flow rate $\dot{V}$, the flow. The valve characteristic factor is considered to be ξ=0.6 due to the sharp reduction of diameter and no rounding of the orifice [Pedersen, 2010]. This assumption has to be made due to the lack of values for comparable situations. The density of the oil is given with $\rho_0 = 890\frac{kg}{m^3}$ [Castrol 2015]. A is the area of ΔK.

3.8 Joining Subsystems

The parts described in the previous sections are now integrated. The power is transmitted from the outer to the inner wheel via the springs. They are fixed by their ends to the outer wheel. They push the inner wheel with their tips. Therefore the main power input of the springs is joined with a 0-junction between the outer and the inner wheel with the power flow in direction to the inner wheel. The bumper is at a similar position and is therefore joined in the same way. The springs also result in a force onto the oil by pushing it with their flanks. Each spring applies pressure to its neighboring oil chambers and the pressures in the chambers counteract with each other. So the second power input of the springs is connected to the respective oil chambers on each side, with the power directing towards the oil.
A preliminary drive train is then added. This "drive train" is an Se-element that is modified by a sine-signal. The preliminary propeller is an R-element with an arbitrarily chosen load of 10^6N. This is used to investigate the properties of the coupling in a less complex setting. As input value the maximum amplitude is set to be the nominal torque. This model now represents a combination of a full coupling and a twelfth of the springs and oil.

3.9 Section counterbalance

There must be a counterbalance for the fact that only a twelfth of the springs and oil chambers are modeled. To achieve this, the sections are regarded as parallel, identical springs. If only one of them is regarded, the power input has to be divided equally between them. They would also give the same power output and vibrations. Therefore, the effort must be multiplied by the number of sections at the output to model the full coupling.

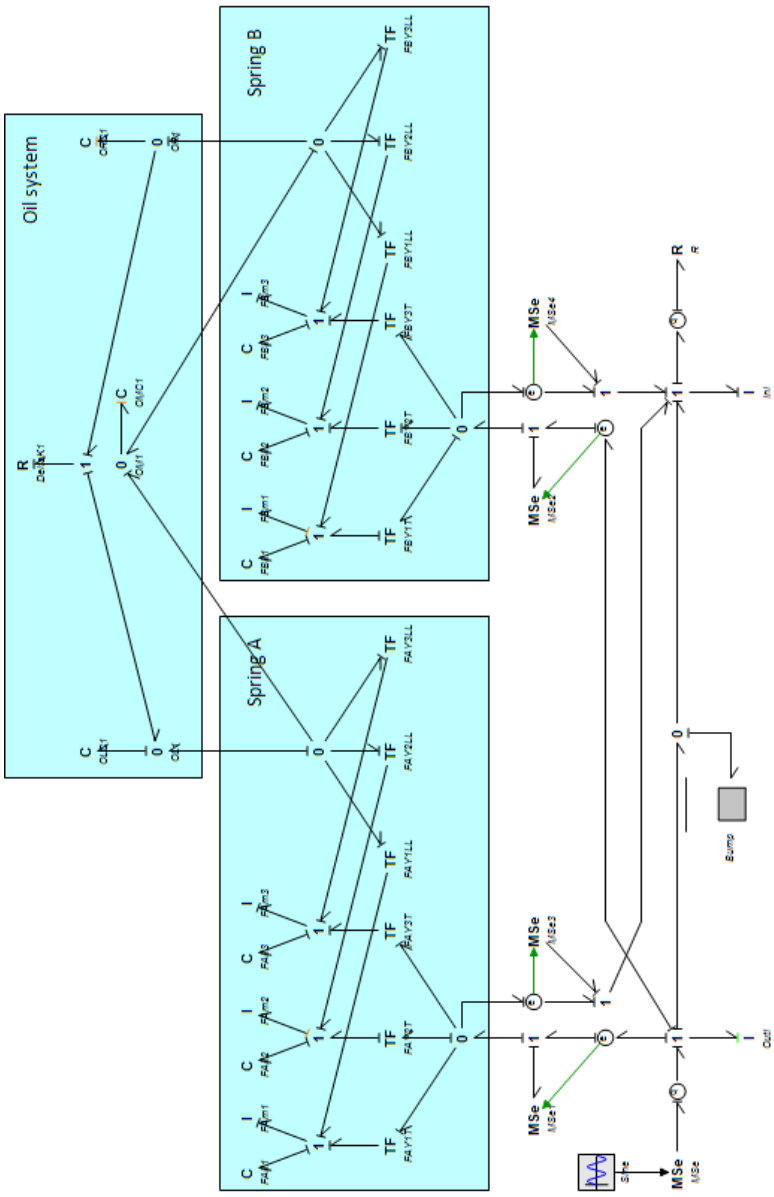

Figure 3.6: Final coupling model

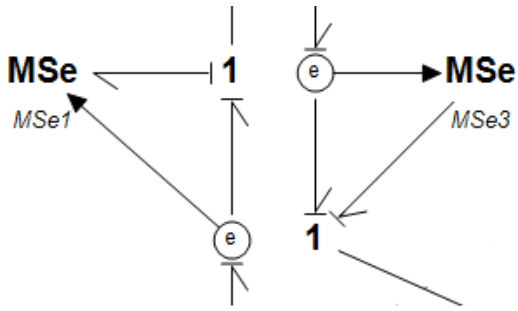

Figure 3.7: Section counterbalance by MSe-elements

Effort- sensors are placed in the power input and output bonds of the springs. Behind that, a 1-junction is added. The sensor signal goes into an MSe-element. A power bond is added between the 1-junction and the MSe-element. The power goes into the source at the input and out of it at the output. The sources take 11/12th of the effort input away and add the 11-times the output effort at the output.

Since the oil chambers are only connected to the springs, this modification adjusts their number as well. This modification is tested. To do so, the coupling is subjected to a constant excitation force of 218kNm at the outer wheel and the inner wheel is fixed with a Sf-element set to zero. Afterwards the MSe-elements are deleted and the simulation is repeated.

With the MSe-elements the force is divided between the one modeled section and the 11 imaginary. Therefore the force acting on the springs and also the displacement are smaller. This can be seen in the following graphs. With the MSe-element for the force adjustment, the displacement is 1/12th of the value that it is without them.

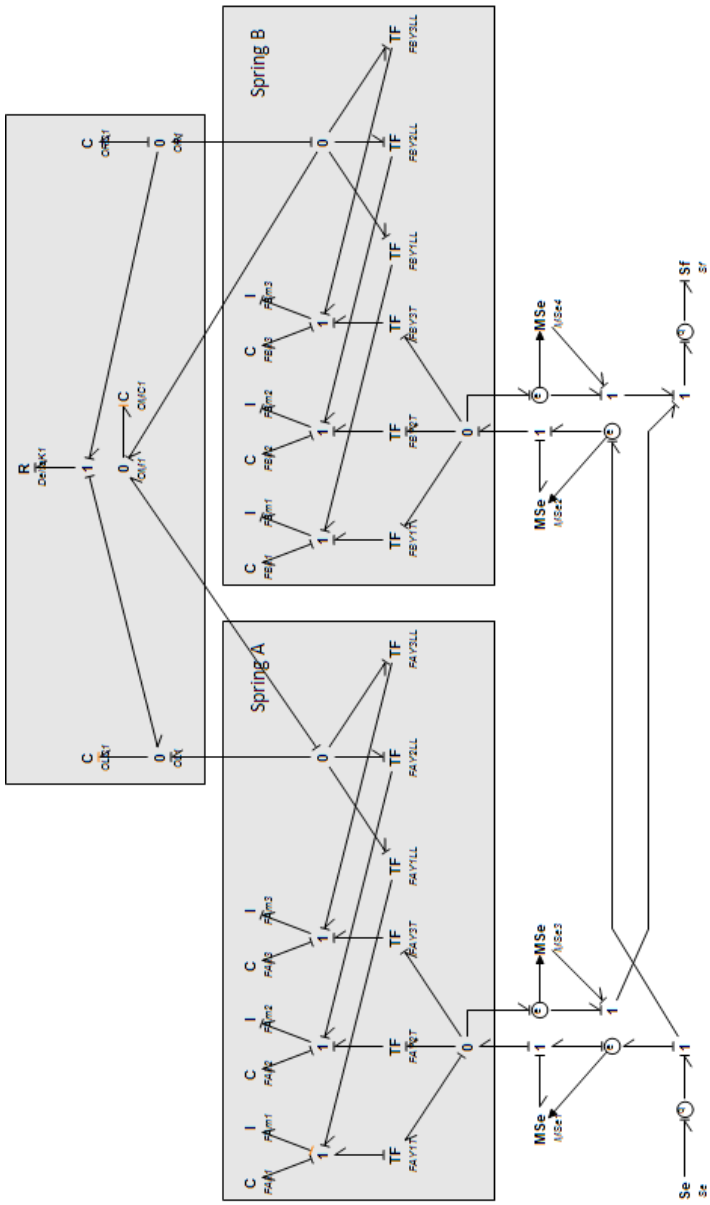

Figure 3.8: Model with fixed inner wheel

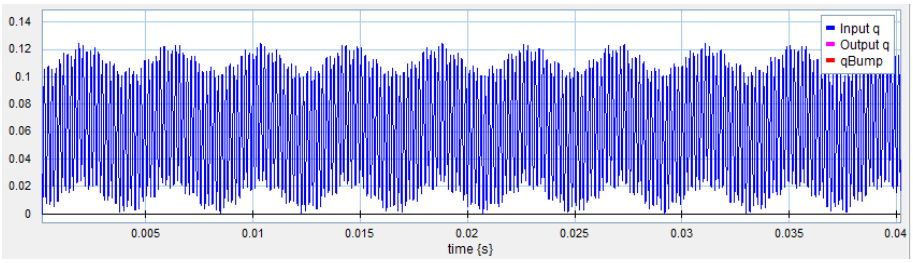

Figure 3.9: Model without MSe-Elements

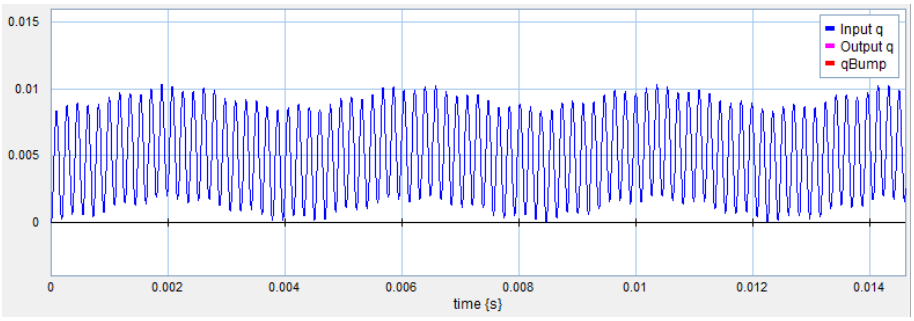

Figure 3.10: Model with MSe-Elements

Chapter 4

Comparison between model and given data

The following data is given for the actual coupling [Geislinger, 2014]:

- Nominal torque T_{KN}= 218 [kNm]
- Static torsional stiffness C_{TStat}=4.78 [MNm/rad]
- Characteristic frequency of coupling ω_0= 690 [rad/s]

4.1 Stiffness

To compare the couplings, the model is subjected to the nominal torque as a static force. The resulting torsion is $5.222.10^{-3}$rad. This results in a static stiffness of 41.74MNm/rad. This means that the static stiffness of the model would be higher than the given value of 4.78 MNm/rad. As this deviation is too high, the stiffness of a single spring is calculated. The spring is again seen as a cantilevered beam that is subjected to a force pushing on the tip. The following values are used for the calculations:

With the following formulas from [Richard, 2008]:

$$I = \frac{h \cdot b^3}{12} \tag{4.1}$$

Table 4.1: Spring calculation values

Name	Source	Symbol	Unit	Value
Nominal Force	[Geislinger, 2014]	F_n	Nm	218000
Number Springs		n_s		24
Length spring	[Vik, 2014]	l_s	m	0.372
Height spring		h	m	0.0315
Breadth spring		b	m	0.1
E-modulus	[DEW, 2015]	E	Pa	$2.1 \cdot 10^{11}$
Diameter inner wheel	[Geislinger, 2014]	D	m	0.29
Factor U to rad	[Convertworld, 2015]			6.28

$$v_L = \frac{F \cdot l_s^3}{3 \cdot E \cdot I} \tag{4.2}$$

a deflection of $2.85 \cdot 10^{-3}$m is calculated. This equals $1.96 \cdot 10^{-2}$rad if the inner diameter of the inner wheel is taken. However, from the drawings it can be seen that the diameter of the wheel at the spring tip is a wider. For this area, the manufacturer doesn't provide a diameter. This gives a stiffness of 0.462 MNm/rad for a single spring and a stiffness of 11.1MNm/rad for all 24 of them. If a bigger diameter for the inner wheel is assumed, this value would be even bigger. Since the springs themselves are 2.3x stiffer than the whole coupling, it is assumed that the springs need to be adjusted to give the coupling a behavior closer to the manufacturers data. This is regarded more closely in the chapter parameter manipulation.

4.2 Eigenfrequency & Dynamic stiffness

The eigenfrequency and the dynamic stiffness of a system depend on each other.

4.2.1 Given values

The dynamic stiffness can be calculated with the following formula [Geislinger, 2014]:

$$0 \leq \omega \leq \omega_0 : \quad C_{Tdyn} = C_{Tstat} \cdot \left(1 + 0.37 \frac{\omega}{\omega_0}\right) \tag{4.3}$$

$$\omega_0 \leq \omega : \qquad C_{Tdyn} = C_{Tstat} \cdot \left(1.1 + 0.27\frac{\omega}{\omega_0}\right) \tag{4.4}$$

This results in these values:

Table 4.2: Dynamic stiffness as a function of frequency

Frequency	C_{Tdyn}	Frequency	C_{Tdyn}	Frequency	C_{Tdyn}
1	4.783	70	4.959	140	5.139
10	4.806	80	4.985	150	5.164
20	4.831	90	5.011	160	5.190
30	4.857	100	5.036	170	5.216
40	4.883	110	5.062	180	5.241
50	4.903	120	5.088	190	5.267
60	4.934	130	5.113	200	5.293

Based on these values the eigenfrequency of the system can be calculated with the following formulas [Schweizer, 2014]:

$$f_K = \sqrt{\frac{C_{Tdyn}}{\sum J_P} \cdot (m+1)} \tag{4.5}$$

$$m = \frac{\sum J_P}{\sum J_L} = \frac{J_{Eng} + J_{OW}}{J_{Prop} + J_{IW}} \tag{4.6}$$

If the manufacturer's values are inserted, this leads to an eigenfrequency between 482.5rad/s for f=1rad and 507.6rad/s for f=200rad. These values are lower than the given frequency of 690rad/s. This can be explained by the lack of inertia from the rest of the power train. The values of J_{Eng} and J_{Prop} would influence the eigenfrequency but they are momentarily set to zero. This has to be kept in mind for the measured values. The higher stiffness of the system would however lead to a higher natural frequency.

4.2.2 Measured values

The eigenfrequency of the model was determined by a Fast-Fourier-Transformation (FFT). This operation is provided within the 20-sim simulation tool. The simulation is performed with an excitation frequency of 150rad/s, an amplitude of

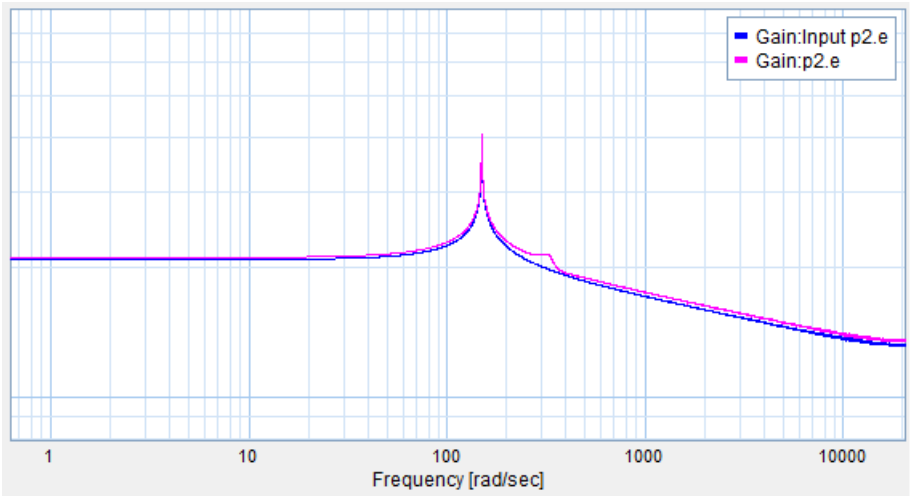

Figure 4.1: FFT Plot of outer and inner wheel torque

6, a peak value of the nominal torque 218kNm and a simulation duration of 10s. In the resulting plot, a distinctive peak of both values at 150rad/s can be seen. Another peak is at 332rad/s for the output torque p2.e. This is the eigenfrequency of the system. Compared to the calculated results in the chapter above, a higher value was expected. The values for the Inertia are the same as in the calculation, which explains why the frequency is lower than the given value. However, the stiffness of the modeled coupling is higher than the calculation values which should result in a higher eigenfrequency than the calculated value.

For another frequency test, the linearization function of 20-sim is used. Therefore the model is subjected to a static excitation force of 218kNm. As input the Se-elements torque is used, as output the q-sensor "output" torque. The resulting torque is 328rad/s, which confirms the finding of the FFT analysis. If this excitation frequency of 330rad/s is inserted into the model, the output torque reaches peak values of 1685kNM. This is 7.7x the input torque. The input displacement reaches 0.041rad. The displacement is mostly damped by the coupling, so that the output displacement is only 0.0011rad.

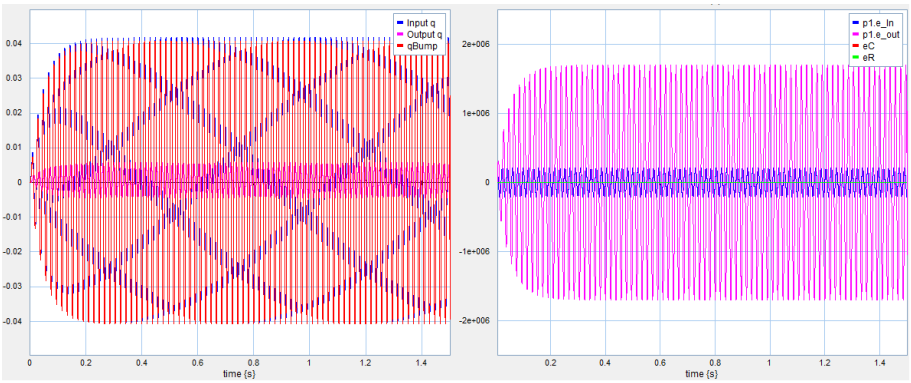

Figure 4.2: Simulation result. Excitation frequency 330rad/s

Chapter 5

Parameter adjustment

As shown in chapter 4, the behavior of the model doesn't match the values provided by the manufacturer. Therefore, the parameters of the model are modified to possibly get a more realistic model behavior.

5.1 Springs

The calculation of the springs as a cantilevered beams sectin: 4.1 show that the stiffness of the springs alone is $\geq$11MNm/rad. As the springs alone can't be stiffer than the whole coupling, this means that they have to be modified to reach the desired behavior. One possibility is the material properties. The kind of steel is not known, therefore a spring steel with a density of 7430kg/m^3 and an E-modulus of 210GPa [DEW, 2015] was chosen. The density is not included in the calculation of the static stiffness. Therefore it is not further regarded here. However, according to [Föll, 2015], the E-modulus for steel is between 190-214GPa. If the lowest value is inserted into the calculation, the static stiffness sinks to 10MNm/rad.
The second possible variation is the spring dimensions. The actual springs are tapered. The base is 46mm wide and the tip 17mm. For the modeling they are simplified to straight beams with a thickness equal to the average value of 31.5mm. However, it seems likely to the author that the base part would bend less than assumed but the tip part would bend distinctively more. Thereby, the overall deflection would be bigger.
Another effect could be the spring base. The actual spring is longer than the

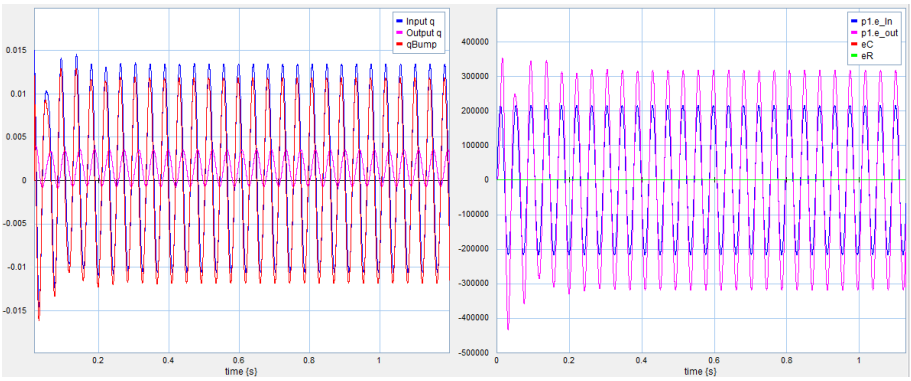

Figure 5.1: Simulation results with modified parameters

used value of 372mm. It has a base that is not taken into account yet because it is pressed against the bumper on one side and can therefore not vibrate freely. It could however have an effect on the spring that should be considered and longer springs would make the model more flexible. The data of the spring dimensions is taken from last year's thesis of Bjørn Eliassen Vik [Vik, 2014] in which the base length is not included. He has the data from an old version of the Geislinger coupling catalogue that is no longer available. Therefore the length must be estimated. It is assumed that the base is longer than wide.
To test the variations, the calculations are inserted into an excel-sheet. After some variations, it is found that 430mm and a thickness of 28.4mm lead to a static stiffness of 4.76MNm/rad. This is considered to be sufficiently close to the given value of 4.78MNm/rad for the whole coupling. The modified values are inserted into the model and simulated in 20-sim with the same basic parameters as in the previous chapter. This results in a deflection of 0.00835rad and therefore a stiffness of 27.25MNm/rad. This is still 5.7x stiffer than the given value. According to the FFT analysis, the eigenfrequency of the system is lowered to 260rad/s. This was expected since a lower stiffness of the system also lowers the eigenfrequency.

5.2 Oil system

With the modified springs, the static stiffness of the coupling is 27.25MNm/rad. Since the springs themselves are now assumed to be less stiff, the oil system is investigated. First the orifice under the bumper is removed. Therefore the 1-junction and the R-element is deleted. This results in a deflection of 0.00822rad and a static stiffness of 26.52MNm/rad. This is 0.73MNm/rad more flexible than the model with the orifice. According to [Geislinger, 2014], the orifice should make the system more flexible and not stiffer. The eigenfrequency according to the FFT-analysis is not affected.
Next, the oil system and the line load on the springs are deleted. Now the simulation time is very long and the bumper is activated during the first oscillations. Therefore the frequency is gradually increased to 180rad/s. At this frequency, the simulation runs smooth again. According to the FFT-analysis, the eigenfrequency is now lowered to 102rad/s which explain why the simulation was not running with a lower frequency. The deflection is now 0.055 which makes the static stiffness 3.964MNm/rad. This is below the given value of 4.78MNm/rad. The aim is to modify the oil system as far as to reach a coupling stiffness that matches the given stiffness. At first the orifice is in the spotlight. The value for the characteristic factor ζ was merely a guess and is therefore modified between 0.5-1. However, this modification doesn't result in any changes of the model's performance.
After a hint form Eilif Pedersen, the bulk modulus β of the oil is taken into consideration. The bulk modulus determines the compressibility of the oil [Watter, 2013]. If the oil is more compressible, the springs can move with less restraint. The bulk modulus is gradually lowered from the original value of 1500MPa, which results in a reduction in stiffness. After some variation, it is found that further reduction of β has a lower effect on the stiffness if $\beta<100$MPa. Therefore the spring thickness was slightly lowered from the modified value of 0.0285m to 0.027m. The sum of these modifications leads to a coupling with the desired static stiffness of 4.78MNm/rad.
However, with this reduction in stiffness comes also a reduction for the natural frequency. The manufacturer's value is f_N=690rad/s, the calculated value is around 500rad/s. The FFT-analysis gives a stiffness of 111rad/s. Because of this, the simulation below isn't performed with a frequency of 150rad/s but instead with a frequency of 50rad/s.

If the orifice is deleted, it has no influence on the stiffness or the natural frequency. This seems rather unlikely to the author. Next the oil system is removed

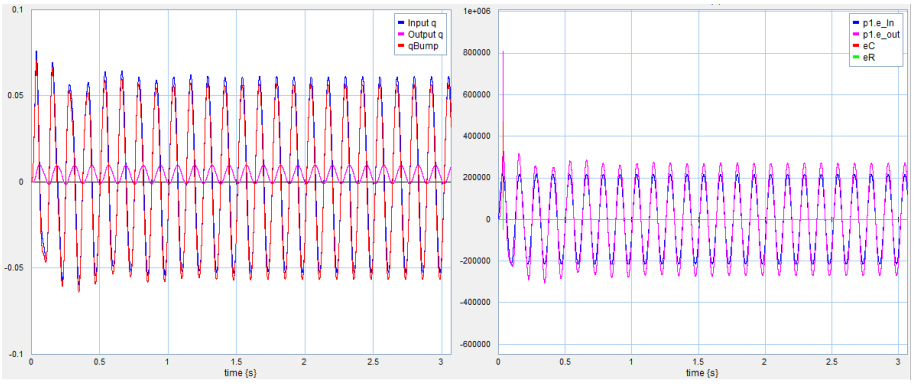

Figure 5.2: Simulation modified coupling excitation frequency 50rad/s

another time to test the changes that occurred due to the further reduction in spring thickness. The static stiffness of the coupling without oil is reduced to 3.46MNm/rad. The natural frequencies are now 10rad/s and 94rad/s.

Chapter 6

Parameter manipulation

It shall be investigated how the model reacts to changes of the parameters that are used in the model. In the previous chapter, changes to the spring dimension and material values as well as the presence or absence of the oil system and its parameters are discussed. In this part, the sensibility of the model to the change of other factors is investigated. This should help to understand the behavior of the coupling better in the more complex setting of the drive train model later. The model used is the coupling with the modified parameters as stated in the end of the previous chapter. The manipulation is performed with the parameter sweep function of the 20-sim simulation program. The simulation is performed several times in a row and one parameter at a time is changed between the runs. The first run is performed with the lowest value chosen and the last with the highest. The first runs appear in a light color and the last in a bold color. It was not possible to change the colors within the graph.

6.1 Excitation frequency

The excitation frequency is varied. Due to the eigenfrequency of the model of 111rad/s, it is not possible to simulate the model between 50-180rad/s excitation frequency. Therefore, two parameter sweep runs are simulated: The first with values between 10-50rad/s, the second between 180-300rad/s.
In the first run, the displacement is quite high in the beginning with values up to 0.07rad/s for the input. The output displacement is also quite high which means that the damping is reduced. With the next step the displacement is

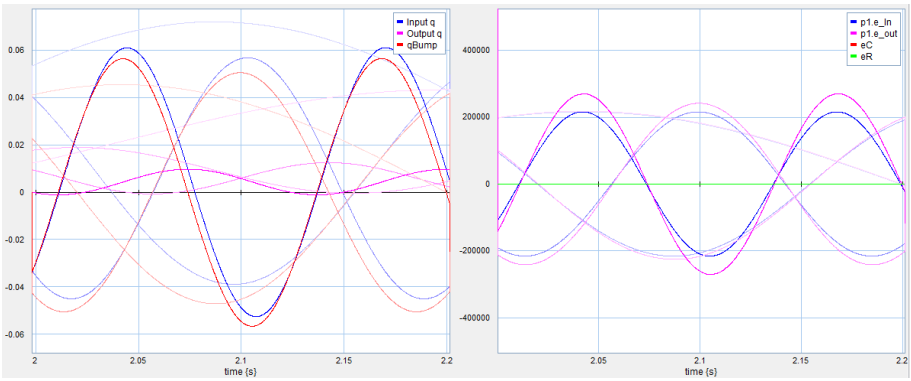

Figure 6.1: Parameter sweep simulation. Frequency variation from 10-50rad/s

lower. At the following step this is turned and the displacement grows again. This happens also at the last step with the peak for the input at 0.06rad/s. The output values however are getting lower throughout the changes and end with a peak value of 0.01rad/s at 50rad/s excitation frequency. This equals a damping of 83.3%. The input torque is constant with a peak of 218kN, the output torque changes. At 10rad/s, the output torque is equal to the input. With a growing excitation frequency, the output torque grows till it reaches peak values of 290kNm at 50rad/s.

In the second run, the input displacement shrinks continually from 0.03rad/s at 180rad/s to 0.008 at 300rad/s. The same happens with the output displacement that sinks from 0.002rad/s to 0.0008rad/s. This means that the damping sinks from 93.3% to 90% with the higher frequency. The input torque is naturally still the same for all frequencies. The output torque sinks from peak values of 130kNm at 180rad/s to 32KNm at 300rad/s.

As a conclusion, it can be said that the input displacement and the output torque grows when the excitation is approaching the natural frequency. For higher frequencies, it is also assumed that the driven wheel can't follow the driver as well which also leads to a lower displacement. The damping efficiency is better towards the natural frequency. This could also be due to the inability of the driven wheel to follow the large displacements that occur towards the eigenfrequency. Therefore the modeled coupling might have higher damping

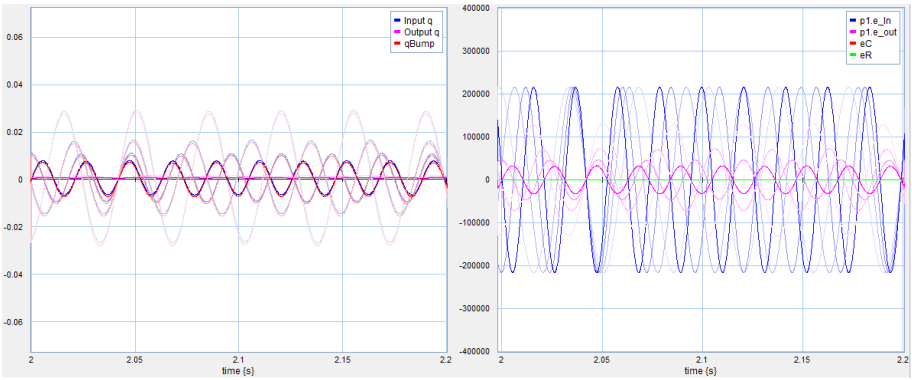

Figure 6.2: Parameter sweep simulation. Frequency variation from 180-300rad/s

capabilities in the low frequency area than the actual part.

6.2 Resistance

The resistance of the R-element that represents the propeller was chosen arbitrarily to be 10MN. The parameter sweep runs between 5-15MN at an excitation frequency of 50rad/s. The input displacement is the biggest for the lowest resistance with 0.066rad and sinks from there to 0.059rad for the highest resistance. The output displacement shows an equal behavior. The highest value is found with 0.019rad at 5MN and the lowest with 0.007rad at 15MN. The displacement difference stays roughly the same at 0.055rad. This means that the damping is improving upon a greater outlet resistance. The torque at the inlet as well as the outlet remains the same throughout the different runs with an outlet torque of 270kN at its peaks. The natural frequency remains also the same throughout the different runs. The run is repeated at 200rad/s excitation frequency and shows the same results. This shows that larger displacements are possible if the resistance is lower.

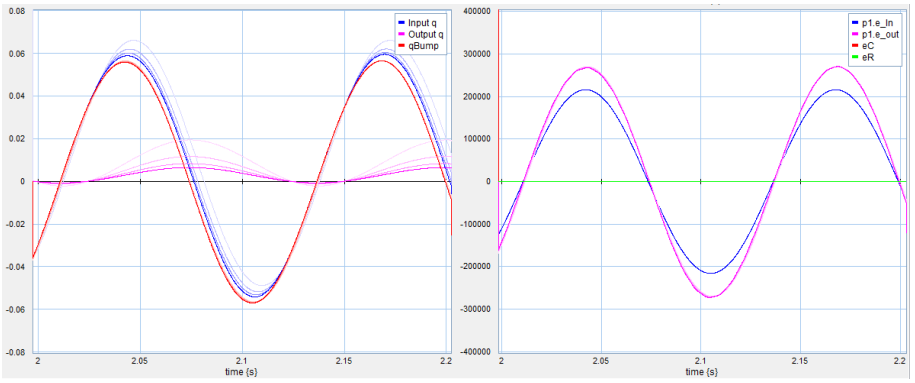

Figure 6.3: Parameter sweep simulation. Resistance variation from 5-15MN at 50rad/s excitation

6.3 Inertia

The inertia of the model is varied. The lower and upper values are chosen from the next coupling sizes in the catalogue: BC 100/10/45 and BC 125/10/45 [Geislinger, 2014]. For the outer wheel, the lower value is 243kgm² and the higher 640kgm². The usual value is 385kgm². For the inner wheel, the range is 12.7kgm² - 40kgm² with a usual value of 21.7kgm². At first, only the outer wheel inertia is varied, then the inner wheel and last both synchronously. The simulation is performed at 30rad/s, as a simulation with 50rad/s was aborted for the higher values. The input displacement is with 0.055rad the lowest for the smallest inertia and grows to 0.059rad for the highest. The output displacement grows in the same direction but with less variety. The lowest value is here 0.0147rad and the highest 0.0153rad. The difference between them also behaves that way with the lowest peak at 0.047rad and the highest at 0.051rad. The damping ratio is similar and varies from 85.5% for the lowest value and 86.4% for the highest.

The FFT analysis shows that the eigenfrequency is influenced by the variation of the inertia. For the lowest outer wheel inertia, the eigenfrequency is 140rad/s. Then it sinks continuously to 86rad/s for the highest inertia. This explains why it was not possible to perform the parameter sweep at 50rad/s as this is too close to the eigenfrequency. It also explains the higher displacement values for

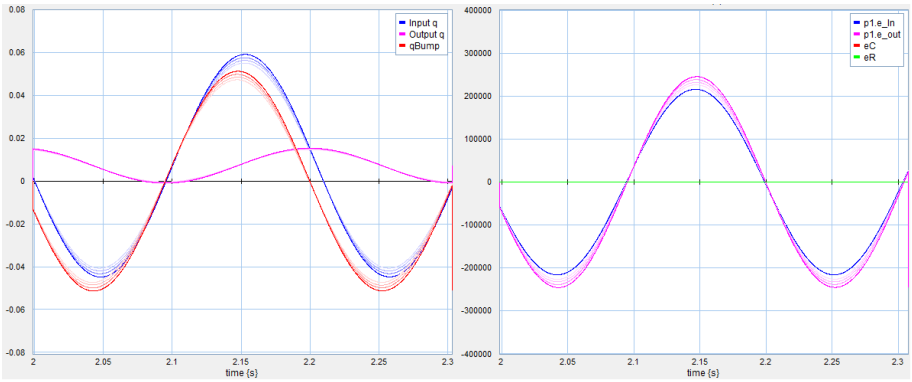

Figure 6.4: Parameter sweep simulation. Outer wheel inertia variation from 243-640kgm^2 at 30rad/s excitation frequency

the system is closer to the eigenfrequency if the input inertia is higher. This behavior can be explained by the formula for the eigenfrequency in which the Inertia is included in the denominator and therefore reduces it upon growing. This leads to the prediction that the eigenfrequency will grow for higher values of the inner wheel inertia. However, when the inner wheel inertia is varied, the results show no variation for any of the observed values. Therefore the parameter sweep is repeated with values between 5kgm^2 to 300kgm^2 but still no variations are found. The FFT-analysis gives the same result. If the outer and the inner wheel inertia are varied parallel, an interesting result is shown. The displacement values for all runs are equal with 0.053rad for the outer wheel, 0.0144 for the inner wheel and 0.045 for the difference between them. The torques are also equal with 218kNm for input as well as the output.

However, the FFT-analysis shows a variation in the eigenfrequency. For the lowest inertias, the eigenfrequency is 538rad/s and 333rad/s for the highest. Even the lowest of these values is three times as high as the usual value of 111rad/s. The parameter sweep is repeated with 200rad/s frequency. The input displacement grows from 0.053rad for the lowest inertias to 0.063rad for the second highest. During the highest inertia run, the twist limiting bumper that is activated at 0.07rad, is hit regularly. The output displacement is stable at 0.0022rad. This means that the damping is better for the higher twist. The input torque is stable as usual and the output torques grow from 243kNm

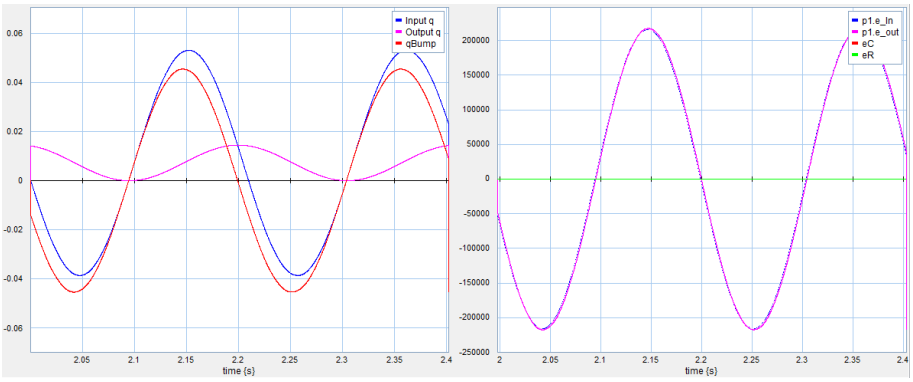

Figure 6.5: Parameter sweep simulation. Outer wheel inertia varies from 243-640kgm² and inner wheel inertia from 12.7-40kgm² at 30rad/s excitation frequency

in the first run to 293kNm in the second last run. During the last run, the repeated bumper activation results in an unstable torque output. The FFT-analysis shows no clear picture of the eigenfrequency as there are too many peaks to distinguish between them. An agglomeration however can be seen around 400rad/s.

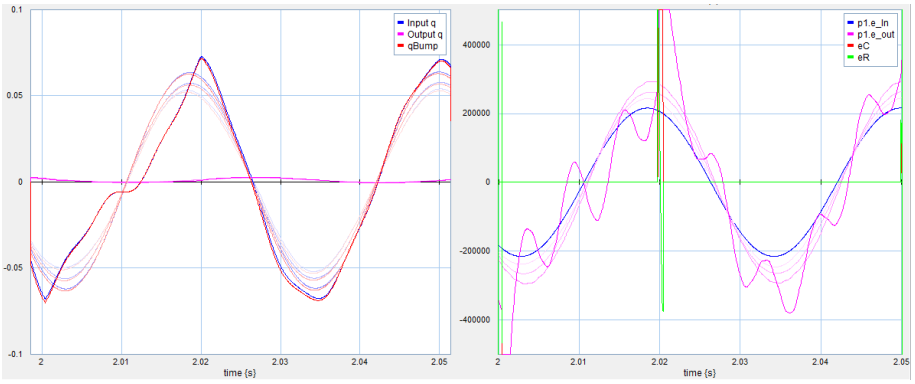

Figure 6.6: Parameter sweep simulation. Outer wheel inertia varies from 243-640kgm² and inner wheel inertia from 12.7-40kgm² at 200rad/s excitation frequency

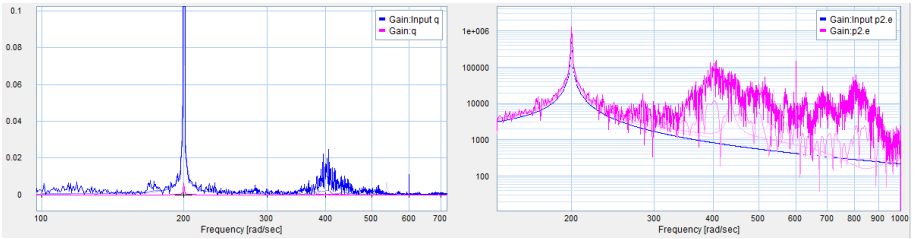

Figure 6.7: FFT-analysis. Outer wheel inertia varies from 243-640kgm² and inner wheel inertia from 12.7-40kgm² at 200rad/s excitation frequency

Chapter 7

Simulation of complete drive train

Finally, the coupling model is inserted into a drive train model. The drive train model is provided by Eilif Pedersen. It represents a 6-cylinder two stroke engine with 0.6m cylinder diameter and a maximal angular velocity of 11rad/s (=105rpm). The power output is not provided but instead determined in the simulation. The dynamic model of the propeller shaft is deleted because the shaft can be considered stiff in comparison to the coupling.

7.1 Comparison of Couplings

In this chapter, two coupling types will be compared. The one, which is explained in the previous chapters and another, simpler one, that merely consists of a C- and an R-element. They are both based on the values of the Geislinger coupling model BC 110/10/45 UC/L. However, for the first (C-complex), the drawings and dimensions are used to create a model that matches the specifications, for the latter (C-simple), the specifications are simply inserted into corresponding elements. This is 4.78MNm/rad for the C-element and 9.711kNms/rad for the R-element [Geislinger, 2014]. First C-simple is tested in the same way as C-complex before: With an MSe-Element generating a sinus wave on one end and an R-element on the other; both with the same parameters as in the previous simulation:

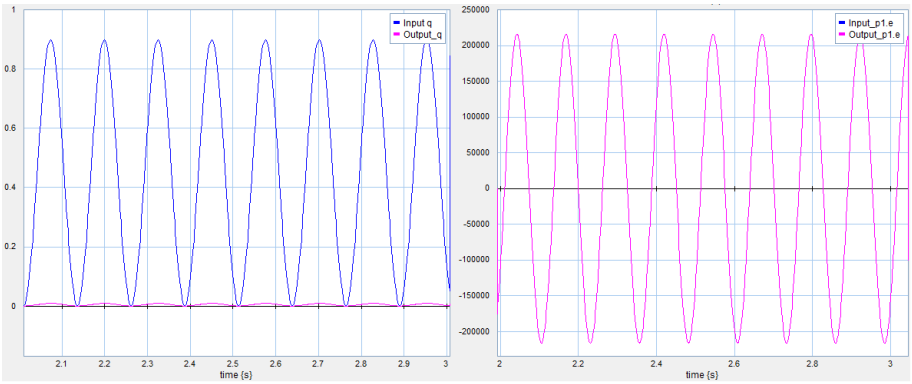

Figure 7.1: C-simple simulation with 50rad/s excitation

- Peak torque: 218kNm
- Frequency: 50rad/s
- Resistance: 1MN

The result shows distinctive differences to the simulation with C-complex that can be seen in chapter "parameter adjustments". The curves are regular sinuses that show no variety over the course of the run whereas C-complex shows higher displacement peaks in the beginning. The maximal displacement of the input is 0.896rad. This is 14.6x as much as the corresponding value from C-complex with 0.061rad and 12.8x the maximal torque of 0.07rad. The output torque is 0.0086rad which is 0.88x the value from C-complex with 0.0097. In C-simple, the output displacement is not delayed unlike to C-complex. C-simple doesn't have an influence on the output torque. It is always equal to the input. In C-complex, the output torque peaks are with 270kNm higher than the input.

It can be concluded that the two couplings show a different behavior under basic conditions. C-simple has the following properties:

- Constant stiffness and resistance at all frequencies
- Greater deflections
- No twist limiter

- Input and output torque are equal

C-complex:

- The stiffness and resistance change dynamically at different frequencies
- Twist limiter that results in nearly infinite stiffness upon activation
- Difference between input and output torque
- Delay of output values
- Eigenfrequency

The coupling models are compared in two different situations. First in the open water: Here, only the normal propeller resistance and inertia is included. The starting up time of the engine is excluded from the inspection. Then the ice load is added. Both couplings are simulated in both cases and additionally a drive train without a flexible coupling is compared.

7.2 Open Water

7.2.1 No coupling

At first, the drive train model is simulated without a coupling to gain some knowledge about the engine behavior. The model exists now only of the engine and the propeller. There is no shaft between the engine and the propeller. From the flow of the engine, it can be seen that the engine overshoots in the beginning and needs 95s to regulate itself to the maximal revolution speed of 11rad/s. From there onwards, it shows transient oscillations between 10.5rad/s -11.5rad/s. The transient oscillation themselves consists of many small, fast vibrations. The overshooting part shall be ignored in the further investigations because the behavior during the normal open water journey is in the focus of this thesis. Therefore, the further investigations shall only regard the behavior after the 100s mark.

The frequency of 11rad/s is a lot lower than the value used in the previous investigations. The displacement is growing constantly. The effort reaches peak values between 40kNm-47kNm. This is about a fifth of the nominal torque. So the coupling is probably over dimensioned for this engine. The overall course of the effort doesn't reflect the transient oscillation. Upon closer inspection, the

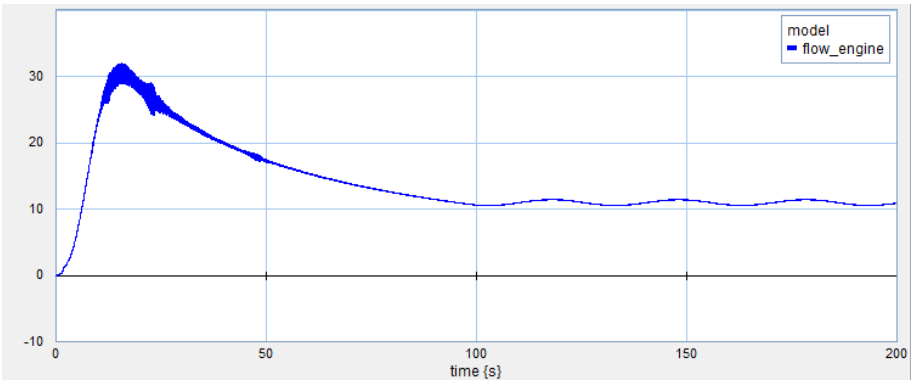

Figure 7.2: Revolution speed in rad/s of engine without coupling

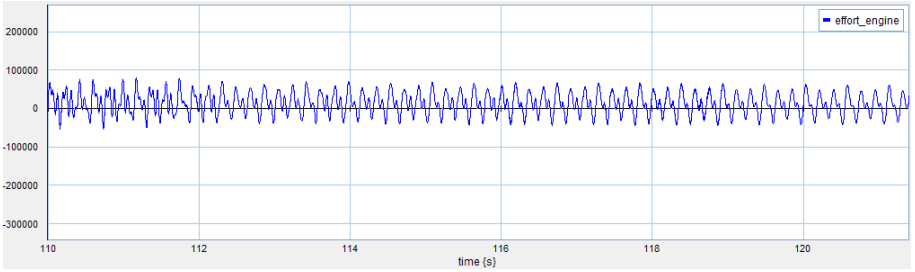

Figure 7.3: Simulation effort engine output of drive train without coupling

effort shows an overlaying of different frequencies, sometimes with many small, fast vibrations and sometimes only few. The power output of the engine shows aspects of both lines, since it comprises of both their input. The peak values of the power range from 490kW – 860kW.

7.2.2 Simple coupling

Next the drive train with the simple coupling. The displacement values also grow linear in this case. Remarkable is the difference between q-engine and q-propeller. After 200s, it has grown to 419rad. This is equal to over 66 complete

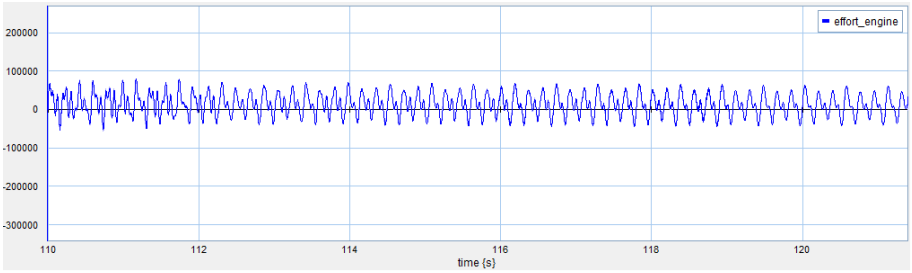

Figure 7.4: Simulation effort engine output of drive train without coupling

revolutions. This would not be possible with a real coupling.

As in the previous simulation of C-simple, there is no difference between the engine and the propeller effort. Compared to the drive train without coupling, the effort is less distributed and the peak values have sunk to less than 12kNm. The effort run shows the large wave pattern from the transient oscillation and consists of fast, smaller oscillations.

The flow of the engine side is similar to the effort. The propeller side also shows the large oscillation but not the faster ones which show that the damping is working for the angular velocity. However, while the engine side sways around 11rad/s, is the propeller side swaying around 10rad/s. This difference explains the displacement difference but this behavior wouldn't be possible for a normal coupling.

The differences in the angular velocity also lead to a power loss over the coupling. For the larger angular velocity, it is around 13kW, for the smaller ones 5.5kW. The relative engine power output is 131kW respectively 81kW. The low power output of the engine and the high losses at the coupling seem unreasonable to the author.

7.2.3 Complex coupling

It is considered that the coupling is located directly behind the engine. Therefore the flywheel inertia is included in the outer wheel inertia.
The displacement difference in this case is vibrating around a point slightly

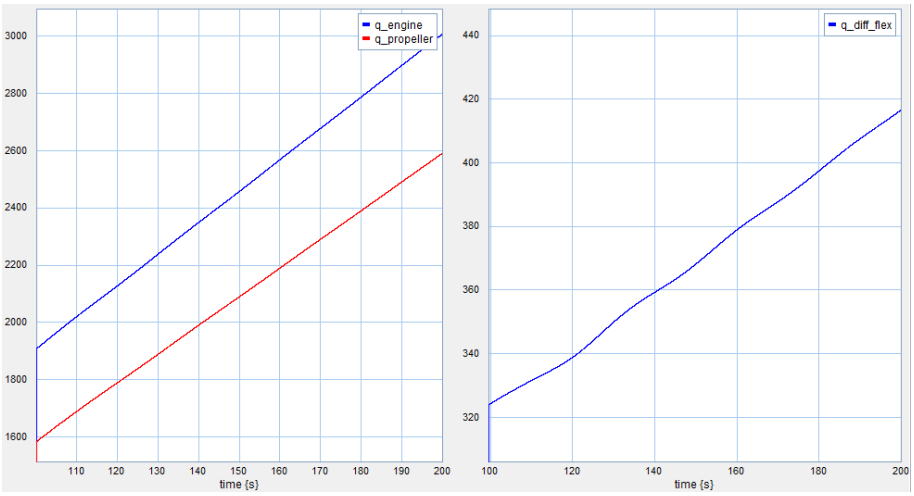

Figure 7.5: Simulation of C-simple. Displacement

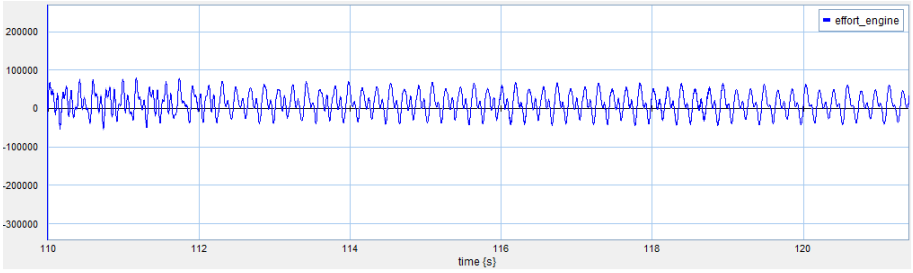

Figure 7.6: Effort output of drive train with Csimple

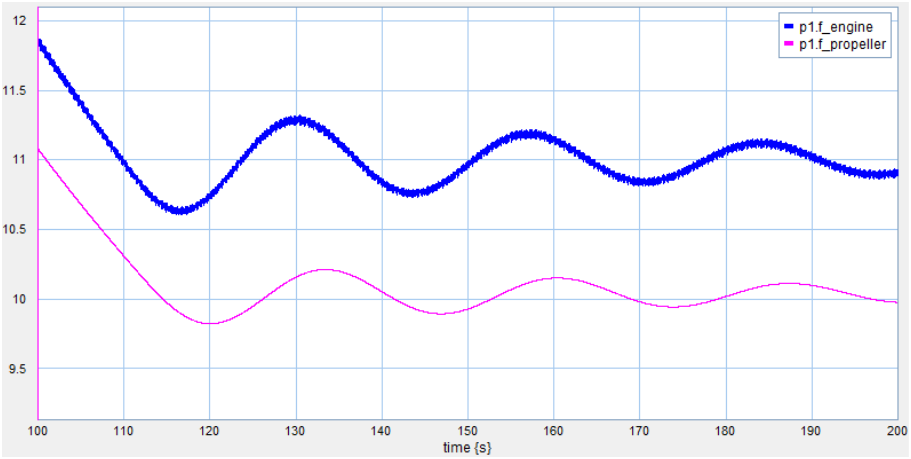

Figure 7.7: Flow output of drive train with Csimple

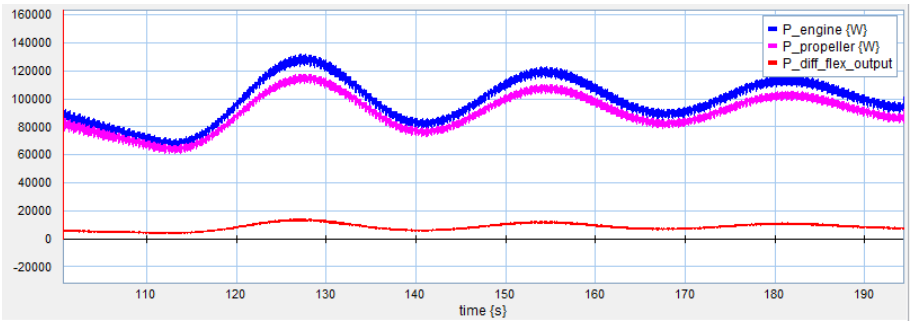

Figure 7.8: Power output of drive train with Csimple

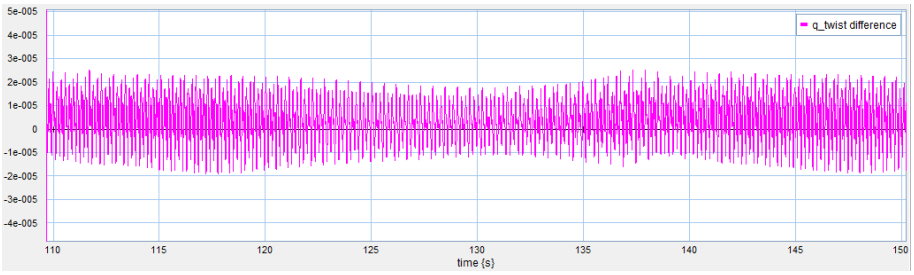

Figure 7.9: Displacement of drive train with Ccomplex

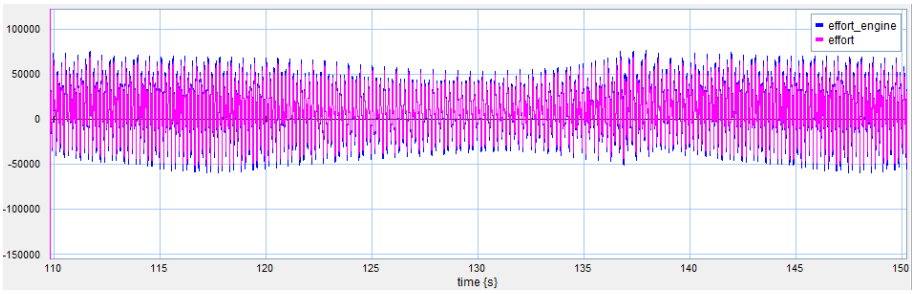

Figure 7.10: Effort output of drive train with Ccomplex

above zero and is never more than $2.5 \cdot 10^{-5}$rad. During the overshooting at the start, top values of 0.004rad are found. The bumper is not activated at any point.

The effort run consists of many fast vibrations but the overall line is straight. However, the amplitude varies. The torque from the engine has peak values around 66kNm and is thereby the highest of all the varieties. The coupling takes the tip off these peaks by reducing them by 5-7kNm. The reduction seems to be higher, the higher the peaks.

The flow shows the same transient vibrations around 11rad/s like the drive train without coupling. The engine and the propeller flow are very similar but upon close inspection, it can be seen that the smallest vibrations are damped out in the propeller flow. The differences between input and output are maximal 0.002rad/s.

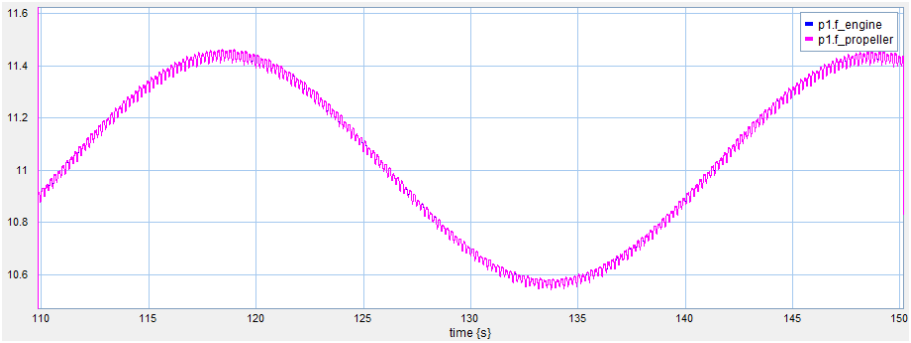

Figure 7.11: Flow output of drive train with Ccomplex

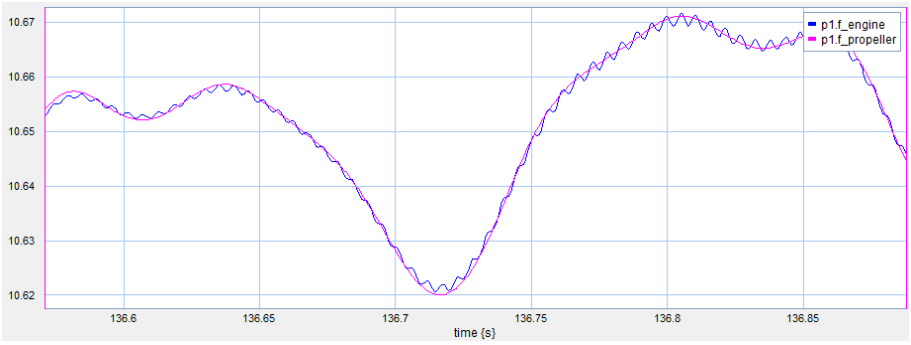

Figure 7.12: Closeup: Flow output of drive train with Ccomplex

The shape of the overall power output is straight but with a varying amplitude. The higher peaks are up to 790kW and the lower peaks around 550kW. The relative power difference of the coupling is around 70kW respectively 40kW.

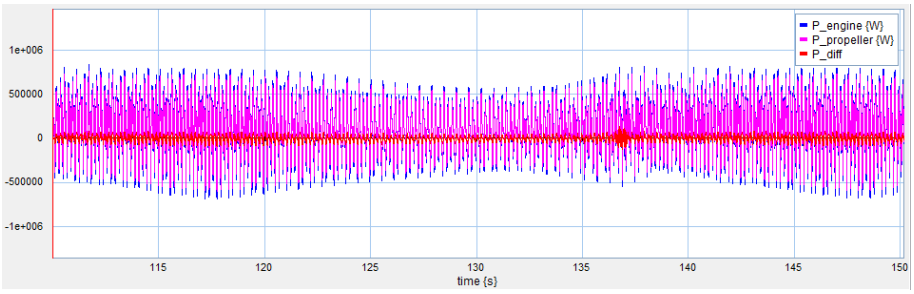

Figure 7.13: Power output of drive train with Ccomplex

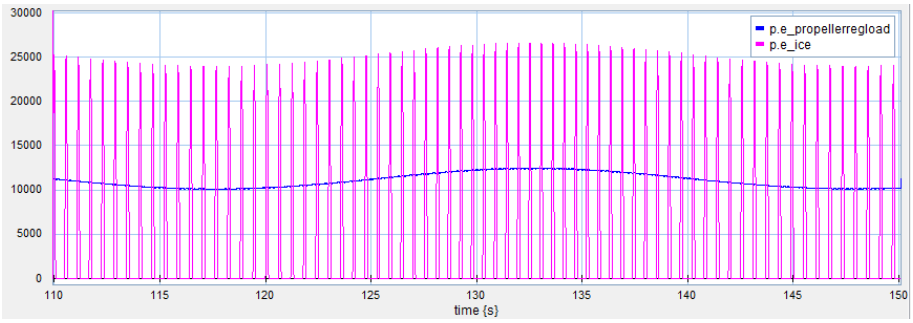

Figure 7.14: Ice load and normal load simulation

7.3 Additional Ice Load

The ice load model from [Polic, 2013] is used. In particular, the case two with the DNV-ice load calculation. It models a single ice block at a time that lead to a half sine shaped load on the propeller. It is inserted as an additional MR-element at the 1-junction of the propeller.

7.3.1 No coupling

The additional ice load forms the expected half sine form with peak values of 251kN. In the displacement, the additional load is not visible. It is still a steady growing function. The effort course is similar to the case without ice. However,

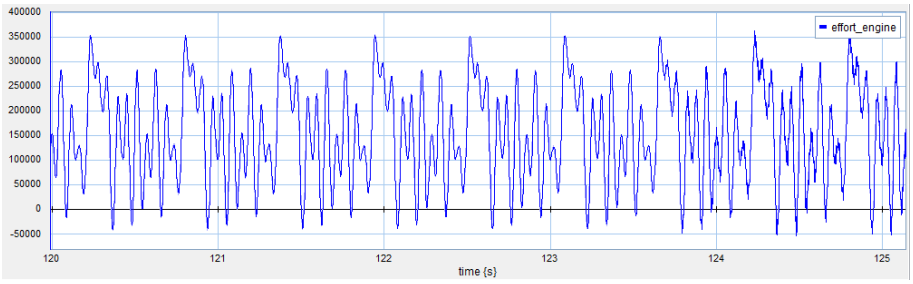

Figure 7.15: Effort of drive train without drive train and ice load

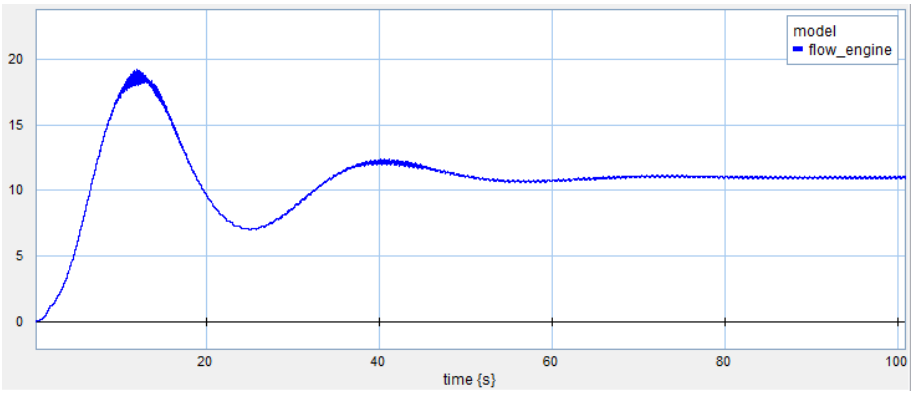

Figure 7.16: Flow of drive train without drive train and ice load

the values are higher than before. The peaks now reach values of 350kNm, before it was around 45kNm.

The flow shows that the engine needs less time to regulate itself. After the overshooting, it reaches its target velocity after 50s run. Without the ice load it needed 95s. The transient oscillations are also reduced. After 70s, the course of the flow is straight. The range of the velocity is slightly smaller than from 10.9rad/s to 11.1rad/s.

The resulting course of the power output is also straight with peak values up to 4000kW. That is 4.5-8x higher that in the simulation without ice load.

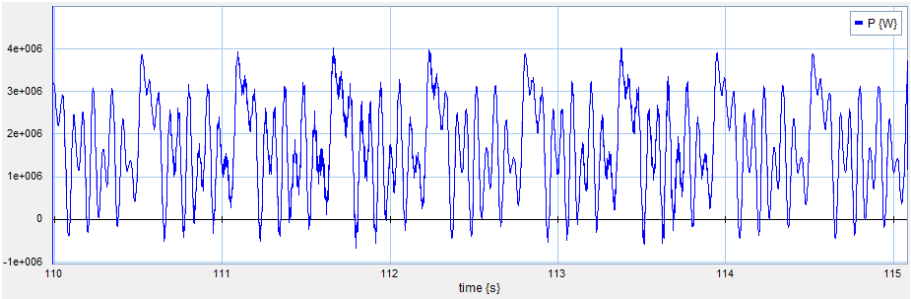

Figure 7.17: Power output of drive train without drive train and ice load

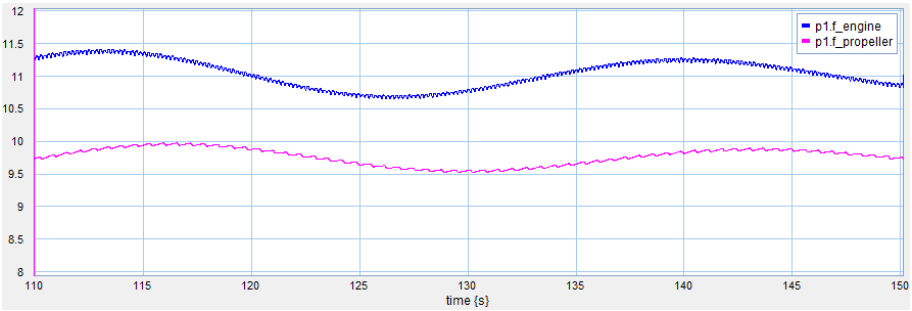

Figure 7.18: Flow of drive train with Csimple and ice load

7.3.2 Simple coupling

In this simulation, there is also a displacement difference comparable to the simulation without ice load, only slightly bigger this time. Before it was 419rad, now it is 460rad at 200s. The gain is linear without oscillations. The flow is similar to the simulation before. It hits the target value at around 94s and continues in transient oscillations. Additional to the behavior without ice, the propeller flow sway now around a slightly lower value of 9.7rad/s and is overlaid with a saw tooth curve.

The transient effort oscillations sway between 10-15kNm.

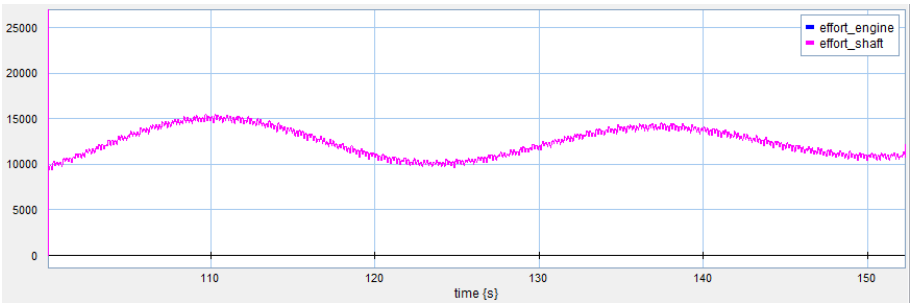

Figure 7.19: Effort of drive train with Csimple and ice load

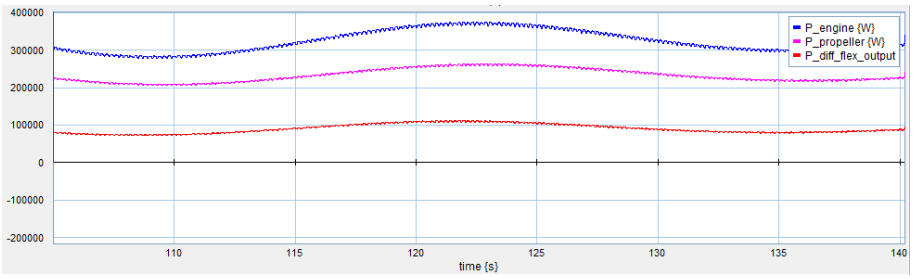

Figure 7.20: Power outpu of drive train with Csimple and ice load

The power output of the engine sways between 95kW-175kW with losses from 10kW-24kW. The faster vibrations at the engine side have an amplitude of 3-4kW, the propeller side is in the same range.

7.3.3 Complex coupling

The displacement difference in this simulation is similar to the one without ice. There are bigger variations in amplitude and the peak values vary from 2.10^{-5}rad -$3.5.10^{-5}$rad. The higher amplitude sections are about 1.10^{-5}rad higher than before.

The effort is also similar to the no ice simulation. Differences can be seen in the

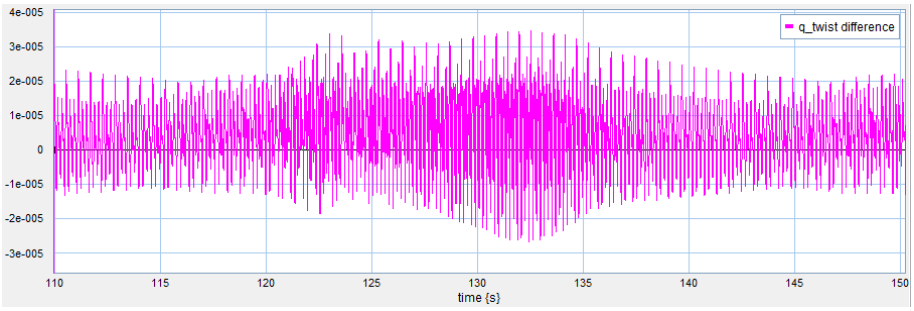

Figure 7.21: Displacement difference of drive train with Ccomplex and ice load

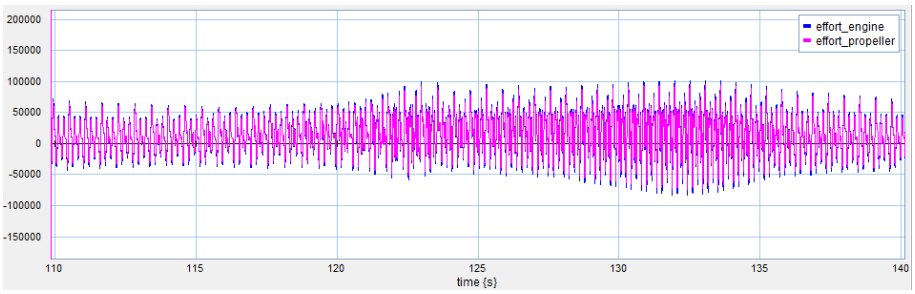

Figure 7.22: Effort of drive train with Ccomplex and ice load

amplitude. The peak values of the engine side range from 55kNm-100kNm. On the propeller side, these peaks are reduced by 3-7kNm.

On the flow side, the impact of the ice load is most visible. While it was perfectly damped in the open water simulation, there is now barely a difference between the two sides. The amplitude of the fast vibrations is now with 0.03rad/s 15x as high as before and upon closer inspection, it can be seen that the now the propeller side is the driving part in these vibrations and that the engine side is slightly damped by 0.002rad/s. The same damping value like before.

Also the power output of the engine is similar to the simulation without ice. There are also sections with higher amplitude. While the low parts are with 550kW equal to the results before, the higher peaks now reach values up to

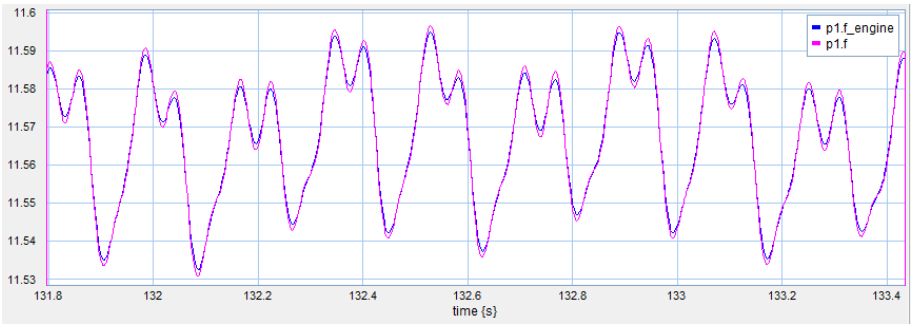

Figure 7.23: Closeup of flow of drive train with Ccomplex and ice load

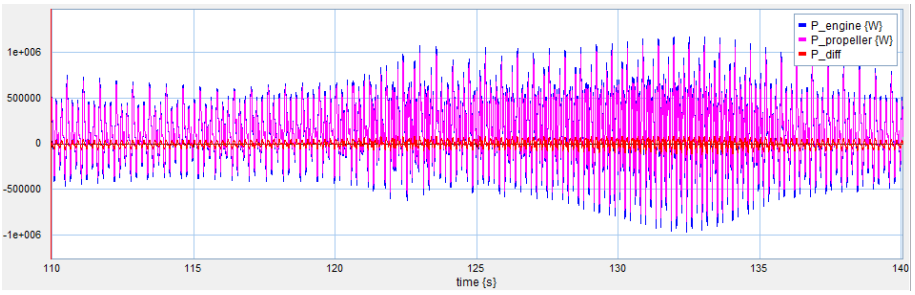

Figure 7.24: Power output of drive train with Ccomplex and ice load

1100kW. The respective power difference is still similar with values between 45-75kW.

7.4 Conclusion

The engine model shows overshooting of the revolution speed and a long phase of transient vibrations. This can be due to a suboptimal engine controller. Another reason could be a too small propeller that doesn't offer enough resistance to the engine. The ice load on the drive train lead to higher peak values for the effort but they are not as distinctive as it was expected from the [Polic, 2013]-paper and the high amplitude have a higher frequency than the ice load peaks. This

amplitude difference can also be seen in the different drive train models. The high amplitude areas could be due to an overlaying of the transient oscillations of the engine and the oscillation of the ice load.
The behavior of Csimple is rather odd. It is unlikely that there are mechanical couplings which allow one side to be constantly 1 rad/s slower than the other side and it would not be possible for the coupling type that is investigated in this thesis. The low effort and the resulting low power output compared to the drive train without coupling and with the different coupling are also remarkable. The effort is 4-7x lower than in the other models. As for the damping, the coupling works well without the ice load. The fast vibrations of the angular velocity are perfectly damped. The damping properties during with the ice load are hard to judge because it has such a small influence on the simulation results.
The behavior of Ccomplex seems more realistic than Csimple. The displacement difference varies around 0 and the flow on the propeller side is on the same level as on the engine side, only damped. The damping is working fine. While the flow is perfectly damped in the open water scenario, the effort is damped by 7-10%.
In the ice load scenario, the damping of the flow has the same value like before but now in the different direction. The larger flow vibrations come from the propeller side and they are transmitted to the engine side. These values are with an amplitude of 0.03rad/s a lot smaller than the transient vibration with 0.5rad/s. The effort difference is reduced to 2-7%. This is unexpected because the torque didn't change during the resistance manipulation tests earlier. The effect on the displacement difference are however as expected, with higher values for the higher resistance of the ice load. The peak values are however still 200x lower than the twist limit. A disadvantage of Ccomplex is the long simulation duration. While the drive train without coupling and with Csimple need less than 4min for a 200s simulation needs Ccomplex up to 1h.

Chapter 8

Results

The results show that the simple, as well as the complex model that are compared in the previous chapter are able to damp the engine vibration towards the propeller side.
As for the ice load scenario, the results are mixed. The suitability of the simple coupling can't be judged by the current results as the effect of the ice load on the simulation output is very limited. The complex coupling showed that the ice load has a vibrating effect that is transmitted to the engine side, despite being slightly damped. However, the effect of the ice load is so little that the transient oscillations of the engine far exceed them. Additionally is the twist limit of the coupling not reached at any point which means that far greater loads could be placed on the coupling The results from section 6.2 suggest that the damping might be better with a greater resistance.
With these results, it seems that there is a mismatch between the engine, coupling and the ice load that prevent sati factionary results. With a softer coupling, the loads from the ice might be damped better by Ccomplex and if the load would be greater, the effect would be better seen in both couplings. As it is now, there are no effects that are expected to be harmful on the engine.
As for the coupling models; both of them have advantages and disadvantages. They both show similar damping capabilities as far as it can be judged. However, the simple model shows a behavior that unrealistic during the open water, as well as the ice load scenario. This can be seen in the flow difference between both sides and the much lower effort values than expected. Ccomplex is more realistic but causes long simulation duration.

Chapter 9

Recommendation for further work

The springs in this thesis are modeled as rectangular beams even though they are in reality tapered. A model that shows the dynamic behavior of tapered spring would probably result in a more realistic behavior of the coupling. Furthermore, some adjustments to the oil system can be tested, in especially the compressibility of the oil and the effect of the orifice. Additionally, a lower simulation time would be useful. To achieve this, it should be tested how simplifications in the model can be done without impairing the accuracy.
To compare a simple coupling with a complex one, it would be good if the simple one shows a more realistic behavior. Therefore Ccomplex should be compared again with a more advanced version of Csimple. Another way to achieve clearer results would be to change some parameters. Another coupling of the same kind but with different dimensions, might be better suited if the load and engine stays the same. A softer coupling would probably perform better in damping out the ice load. Else, the propeller size or the ice strength can be increased to expose the couplings to bigger loads. Then it would be easier to distinguish their respective suitability.

Bibliography

[Borutzki, 2000] Borutzki, W. (2000). Bondgraphen: Eine Methode zur Modellierung multidisziplinärer dynamischer Systeme. Ghent: SCS-Europe BVBA.

[Castrol 2015] Castrol Limited. (n.d.). Castrol Marine Lubricants. Retrieved 03 17, 2015, from http://msdspds.castrol.com/bpglis/FusionPDS.nsf/Files-/2A0C180E868C914180257D6C004C91BC/$File/BPXE-9QPB8T.pdf

[Controllab, 2015] Controllab-Products. (n.d.). 20sim Products. Retrieved 04 15, 2015, from http://www.20sim.com/products/20-sim.html

[Convertworld, 2015] Convertworld. (n.d.). Convertworld.com. Retrieved 06 02, 2015, from http://www.convertworld.com/de/winkel/

[DEW, 2015] DEW, Deutsche Edelstahlwerke GmbH. (2011, 08). Cr-Si-legierter Federstahl: 1.7108, 61SiCr7. Retrieved 05 12, 2015, from http://www.dew-stahl.com/fileadmin/files/dew-stahl.com/documents/Publikationen/Werkstoffdaten-blaetter/Baustahl/1.7108_de.pdf

[Föll, 2015] Föll, H. (n.d.).Christian-Albrecht-Universität Kiel. Retrieved 06 03, 2015, from MaWi1 - Elastizitätsmodul in Zahlen: http://www.tf.uni-kiel.de/matwis/amat/mw1_ge/kap_7/illustr/t7_1_2.html

[Geislinger, 2014] Geislinger GmbH. (n.d.) (2014). Geislinger/Downloads/Couplings. Retrieved 01 20, 2015, from http://www.geislinger.at/assets/geislinger.at//downloads-/Coupling_17.7.pdf

[HUG, 2015] HUG Industrietechnik und Arbeitssicherheit GmbH. (n.d.). HUG Technik Tabellen. Retrieved 03 01, 2015, from http://www.hug-technik.com/inhalt/ta/metall.htm

[Karnopp, 2006] Karnopp, D., Margolis, D., & Rosenberg, R. (2006). System Dynamics, Modeling and Simulation of Mechatronic Systems; 4th edition. Hoboken: John Wiley & Sons, Inc

[Kuiken, 2008] Kuiken, K. (2008). Diesel Engines: for ship propulsion and power plants from 0 to 100,000 kW. Onnen, Netherlands: Target Global Energy Training.

[Meirovitch, 2001] Meirovitch, L. (2001). Fundamentals of Vibration. New York: The McGraw-Hill Companies, Inc.

[Muhs, 2007] Muhs, D., Wittel, H., Jannasch, D., & Voßieck, J. (2007).Roloff Matek - Maschinenelemente. Wiesbaden: Friedr. Vieweg & Sohn Verlag.

[Pedersen, 2010] Pedersen, E., & Engja, H. (2010). Mathematical Modelling and Simulation of Physical Systems: Lecture Notes in TMR4275 Modelling, Simulation and Analysis of Dynamic Systems. Trondheim: Norwegian University of Science and Technology.

[Polic, 2013] Polic, D., Æsøy, V., Ehlers, S., & Pedersen, E. (2013). Propulsion machinery operating in ice - A modelling and simulation approach. Trondheim: NTNU.

[Richard, 2008] Richard, H. A., & Sander, M. (2008). Technische Mechanik - Festigkeitslehre, 2.Edition. Wiesbaden: Vieweg+Teubner GWV Fachverlage GmbH.

[Schweizer, 2014] Schweizer, A. (2014, 12 02). Formelsammlung - Berechnungsprogramme für Anlagenbau und Stromaggregate. Retrieved 05 13, 2015, from Antrieb-Kupplungen: http://www.schweizer-fn.de/antrieb/kupplung/kupplung.php

[Vik, 2014] Vik, B. E. (2014). Master Thesis - Development and Verification of a Gesilinger [sic] Flexible Coupling Bond Graph Model. Trondheim: NTNU.

[Watter, 2013] Watter, H. (2013). Hydraulik und Pneumatik. Wiesbaden: Springer Fachmedien.